Spatiotemporal effects in double phase conjugation

M. R. Belić

Institute of Applied Physics–Nonlinear Dynamics, Technical University Darmstadt, Hochschulstrasse 4a, 64289 Darmstadt, Germany, and Institute of Physics, P.O. Box 57, 11001 Belgrade, Yugoslavia

J. Leonardy

Institute of Applied Physics–Nonlinear Dynamics, Technical University Darmstadt, Hochschulstrasse 4a, 64289 Darmstadt, Germany

D. Timotijević

Institute of Physics, P.O. Box 57, 11001 Belgrade, Yugoslavia

F. Kaiser

Institute of Applied Physics–Nonlinear Dynamics, Technical University Darmstadt, Hochschulstrasse 4a, 64289 Darmstadt, Germany

Received July 25, 1994; revised manuscript received April 4, 1995

Spatial and temporal effects arising in photorefractive crystals during the process of double phase conjugation are analyzed numerically with a novel beam-propagation method. Slowly varying envelope wave equations in the paraxial approximation are solved under the appropriate boundary conditions. Our analysis includes dynamical effects caused by the buildup of diffraction gratings in the crystal and the turn-on of phase-conjugate beams as well as spatial effects caused by the finite transverse spread of beams and by the propagation directions of the beams. Various phenomena are observed, such as self-bending of phase-conjugate beams, convective flow of energy out of the interaction region, mode oscillations, critical slowing down at the oscillation threshold, and irregular spatial pattern formation. For a real beam-coupling constant and constructive interaction of interference fringes in the crystal we find steady or periodic behavior. For a complex coupling constant and/or induced phase mismatch in the grating a transition to spatiotemporal chaos is observed. We believe that under stable operating conditions the transverse double phase-conjugate mirror in the paraxial approximation is a convective oscillator, rather than an amplifier. Improved agreement with experimental results is obtained.

1. INTRODUCTION

Double phase conjugation (DPC) was shrouded in controversy almost from its conception. It is an interesting wave mixing process in which two laser beams illuminate a photorefractive (PR) crystal incoherently, causing the appearance of two counterpropagating phase-conjugate beams (Fig. 1). DPC was suggested and first demonstrated by Cronin–Golomb *et al.*[1] but was deemed improbable by the same group, because of the competing conical emission. Indeed, the initial demonstration was achieved with the use of additional mirrors. It took a few years for Fischer and his colleagues[2] to demonstrate DPC in its pure form, two beams plus a crystal. What made this possible is the preferential amplification of both conjugate beams by a particular set of fanning gratings.

A more recent controversy involving DPC is connected with the question whether DPC is a self-oscillation process or an optical amplification process. The difference between the two is subtle in numerical simulations as well as in experiment. It amounts to whether a finite phase conjugate (PC) output can be obtained from zero (i.e., infinitesimal) input or whether a finite input is always needed. Oscillation requires a fast (exponential) growth rate above threshold and a feedback mechanism. In the plane-wave (PW) case it is agreed that DPC is an oscillation.[2] In the spatial case with one or two transverse dimensions this is not clear. The analysis of Ref. 3, based on a linear, undepleted-pumps theory, indicates that DPCM is a convective amplifier. This was confirmed experimentally by the same group for arbitrary large angles between the interacting beams.[4] A more recent and more comprehensive analysis of a similar theory[5] (including depletion and diffraction) reaffirms that conclusion. Another transverse model[6] based on a PW expansion claims that the double phase-conjugate mirror (DPCM) is still an oscillator. The theory presented in Ref. 7 uses the vectorial nature of coupled-wave equations to show that the DPCM is an oscillator.

Among other things, we try to elucidate this controversy. However, this is not the central theme of this paper. In general, we want to understand the operation of a DPCM and to study its spatiotemporal behavior. A convenient starting point for such a program is the wave equations describing four-wave mixing (4WM) processes in the paraxial approximation:

0740-3224/95/091602-15$06.00

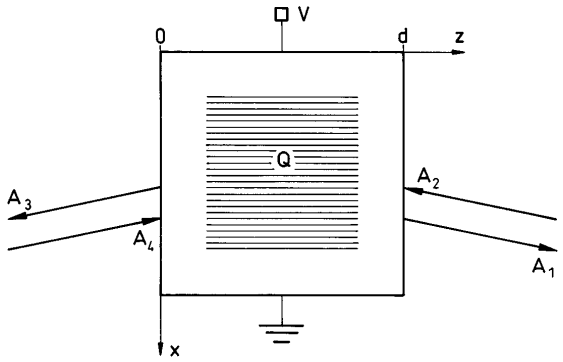

Fig. 1. DPCM. Pump beams A_2 and A_4 enter the crystal from opposite sides. A_1 is the PC of A_2, and A_3 the PC of A_4. z is the propagation direction and x is one of the transverse directions, the other, y, being perpendicular to the $x-z$ plane. Q represents the amplitude of the transmission grating. V is the high-voltage source of the electric field E_0 (see Section 5).

$$\partial_z A_1 + \beta\hat{K}\cdot\nabla_T A_1 + i\phi\nabla_T{}^2 A_1 = QA_4\,, \tag{1a}$$

$$\partial_z A_2 + \beta\hat{K}\cdot\nabla_T A_2 - i\phi\nabla_T{}^2 A_2 = \overline{Q}A_3\,, \tag{1b}$$

$$\partial_z A_3 - \beta\hat{K}\cdot\nabla_T A_3 - i\phi\nabla_T{}^2 A_3 = -QA_2\,, \tag{1c}$$

$$\partial_z A_4 - \beta\hat{K}\cdot\nabla_T A_4 + i\phi\nabla_T{}^2 A_4 = -\overline{Q}A_1\,, \tag{1d}$$

where $A_j(x, y, z)$ are the slowly varying envelopes of the four beams, β is the relative transverse displacement (caused by the noncollinear propagation of the four beams), and ϕ is the parameter controlling the diffraction in the crystal. In scaled coordinates $\beta = \theta/\sqrt{2}\,\delta$, where θ is the half-angle at the beam intersection and δ is the angular spread of the interacting beams. ϕ is proportional to the inverse of the Fresnel number: $\phi = (4\pi F)^{-1}$. $\hat{K}\cdot\nabla_T$ is the directional derivative in the transverse (x, y) plane along the grating wave vector $\hat{K}$, and $\nabla_T{}^2 = \Delta_T$ is the transverse Laplacian. The bar denotes complex conjugation, and Q is the amplitude of the grating that is generated in the crystal. The x and y axes are arranged so that the wave vector of the grating points along the $y = x$ direction. Equations (1) are derived in Appendix A.

To these equations one must specify boundary conditions. The conditions are that the four initial amplitudes C_{1-4} be launched into the crystal, as in Fig. 1. The transverse amplitude profiles are assumed to be displaced Gaussians, with parameters that take into account noncollinear propagation of the beams:

$$\begin{aligned} A_{4,1}(x, y, 0) &= C_{4,1}G(-\zeta, \rho)\,,\\ A_{2,3}(x, y, d) &= C_{2,3}G(\zeta, \rho)\,, \end{aligned} \tag{2}$$

where $z = 0$ and $z = d = 1$ denote the entry and the exit faces of the crystal, respectively, and $G(\zeta, \rho)$ is the Gaussian beam function:

$$G(\zeta, \rho) = \frac{\exp\left\{i\left[\tan^{-1}(\zeta) - \dfrac{\rho^2}{\zeta + \zeta^{-1}}\right] - \dfrac{\rho^2}{1+\zeta^2}\right\}}{\sqrt{1+\zeta^2}}\,. \tag{3}$$

Here $\zeta = 4\xi/F$, where ξ is the beam curvature parameter[8] and F is the Fresnel number. $\rho^2 = [(x \pm \beta/2)^2 + (y \pm \beta/2)^2]/\sigma^2$, where σ is the stretching factor that keeps the transverse computational space between -1 and $+1$. In DPC the initial PC beams C_1 and C_3 are not supplied externally; they arise from the noise in the crystal. Therefore we set C_1 and C_3 very small compared with the pumps C_2 and C_4 (in general smaller than 10^{-4}).

The temporal evolution of Q is approximated by a relaxation equation of the form

$$\tau\partial_t Q + \eta Q = \frac{\Gamma}{I}(A_1\overline{A}_4 + \overline{A}_2 A_3)\,, \tag{4}$$

where τ is the relaxation time of the grating, η is a dimensionless parameter dependent on the ratio of internal electric fields of the PR crystal, I is the total intensity, and Γ is the PR coupling strength (coupling constant times the crystal thickness). Both Γ and β can be positive or negative; however, we consider only the positive values. The waves are following the changes in the crystal adiabatically; therefore the temporal derivatives in Eqs. (1) are ignored. Likewise, the spatial derivatives are neglected in Eq. (4), because the diffusion effects are controlled by the slow electronic processes in PR crystals.

Not many researchers were concerned with transverse and dynamical effects in PR oscillators.[9] Apart from the Russian and American groups cited above,[3–6] Liu and Indebetouw[11] expressed interest in the dynamics of vortices in PR cavities. They employed off-Bragg wave-number mismatch as a means of destabilizing the intracavity oscillation. Another way to destabilize the intracavity field is to apply an external electric field across the crystal, whereby the coupling constant is made complex.[12] We use this method to drive the system to spatiotemporal chaos.

Numerical solution of 4WM problems including transverse and dynamical effects is beyond the reach of present-day computers. To our knowledge this has not been attempted in its full complexity. An approximate method based on a truncated modal decomposition is employed in Ref. 11. The authors decomposed an intracavity field into a small number of Gauss–Hermite modes, hoping to capture the dynamics of modes in the crystal by a limited set of eigenmodes of the empty cavity. Not more than qualitative agreement with experiment can be expected from such a method, especially if there are instabilities and chaos in the system.

Another transverse model, two-wave mixing with truncated PW decomposition, is used to describe PR backscattering, soliton propagation, and DPC.[6] The treatment is restricted to one transverse dimension. Similar in spirit to our method is the whole-beam method presented by Cronin-Golomb and Ratnam and Banerjee.[10] All the interacting beams in that method are treated as one combined beam interacting with itself in the crystal. The method is applied to two-wave mixing in steady state and in one transverse dimension.

We present a novel numerical procedure that is based on the thin gain sheets beam-propagation method (BPM).[13] The method was used originally for mode calculations in high-power lasers, and here it is modified to handle wave mixing in PR crystals. Such mixing permits adiabatic separation of the spatial mode problem in the crystal from the slow temporal problem of the buildup of gratings. This makes the numerical problem tractable.

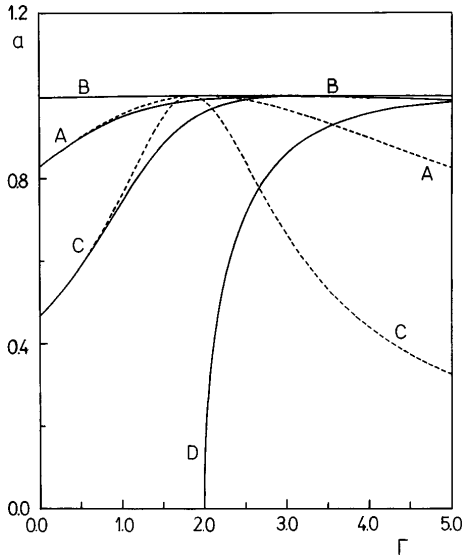

Fig. 2. Self-consistency parameter a as a function of the coupling strength Γ. Solid curves are the numerical solutions of Eq. (B6); dashed curves are the approximate solutions, Eq. (B7). Curves AA and BB are the simple PC curves, with the boundary conditions $|C_1|^2 = |C_2|^2 = 1$, $|C_3|^2 = 0$, and $|C_4|^2 = 0.7$ for the AA and $|C_4|^2 = 0.4$ for the BB curves. Curve CC is the 4WM curve, with the conditions $|C_1|^2 = 0.4$, $|C_2|^2 = 1$, $|C_3|^2 = 0.1$, and $|C_4|^2 = 1$. Curve D is the DPC threshold curve, Eq. (7), with the conditions $|C_2|^2 = 1$, $|C_4|^2 = 0.1$ (arbitrary units).

However, instead of treating all interacting beams as one whole beam, or making PW or other truncated decompositions of beams, we retain the individuality of all four beams. We perform mostly three-dimensional simulations and include temporal variations. The procedure is checked in parts and as a whole on analytical and numerical PW results, to yield good agreement. In treating transverse effects we concentrate on the influence of diffraction because the effects of noncollinearity have been thoroughly investigated by others.[3] In treating dynamical effects we concentrate on the behavior that leads to instabilities and spatiotemporal chaos.

This paper is organized as follows. Section 2 presents the PW theory of DPC. A numerical method for solution of Eqs. (1) and (4) is presented in Section 3. Section 4 deals with the spatial aspects of the generation and propagation of PC beams in the crystal. Section 5 is concerned with the dynamical effects connected with DPC, including spatiotemporal instabilities. Section 6 provides discussion and offers some conclusions.

2. PLANE-WAVE THEORY

Analytical treatment of Eqs. (1) and (4) is not possible. Equations without diffraction ($\phi = 0$) have been considered in Ref. 3. Steady-state PW absorptionless 4WM equations were first considered by Cronin-Golomb *et al.*[1] The case of real coupling constants was treated in Ref. 14. We follow that method. The solution procedure is outlined in Appendix B.

For DPC boundary conditions are simplified, in that $C_1 = 0$ and $C_3 = 0$. This leads to a simplification in the solution procedure of Appendix B. The exit PC fields [from Eqs. (B2)] are given by

$$A_{30} = C_2 \sin(u), \qquad A_{1d} = C_4 \sin(u), \tag{5}$$

where $u = \Theta_d - \Theta_0$ is the total grating action. The boundary values Θ_0 at $z = 0$ and Θ_d at $z = d$ of the independent variable $\Theta(z)$ from Appendix B are given by

$$\tan(\Theta_0) = \exp\left(-\frac{a\Gamma}{2}\right)\left(\frac{a - q^*}{a + q^*}\right)^{1/2},$$
$$\tan(\Theta_d) = \exp\left(\frac{a\Gamma}{2}\right)\left(\frac{a - q^*}{a + q^*}\right)^{1/2}, \tag{6}$$

where $q^* = (|C_4|^2 - |C_2|^2)/(|C_4|^2 + |C_2|^2)$ is the ratio of the input power flux to the total input intensity. The self-consistency parameter a is found from the transcendental equation

$$a = \tanh(a\Gamma/2). \tag{7}$$

This is an important parameter in the theory. It defines the threshold for oscillation. A sample of values for different wave mixing processes is depicted in Fig. 2. The

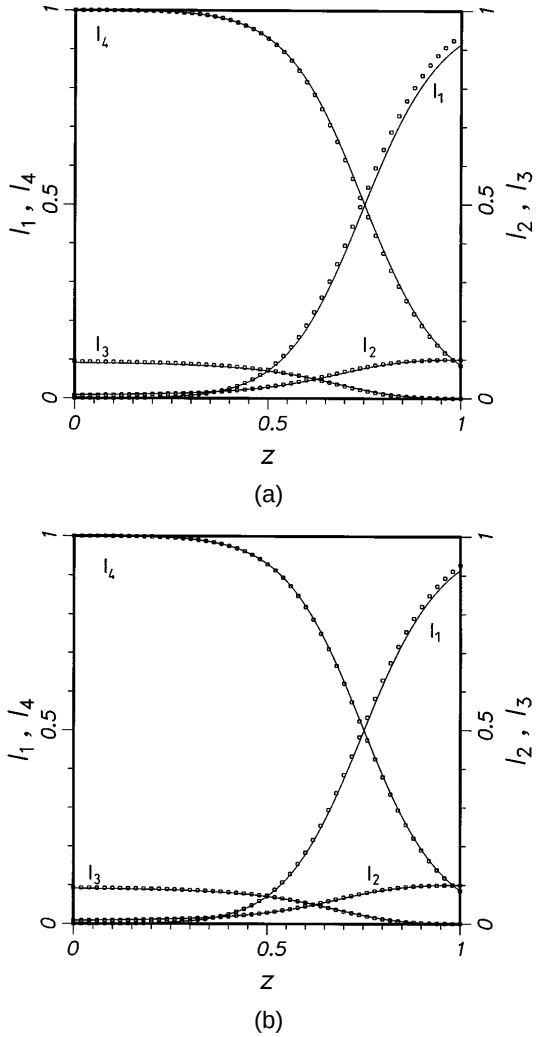

Fig. 3. Checking the numerics: comparison with PW solutions (curves, analytical results; squares, numerical results). Four fields inside the crystal are shown as functions of the longitudinal spatial variable z. (a) $\delta z = 0.01$, (b) $\delta z = 0.005$. In the following computations δz is kept fixed at 0.005. The other parameters are $\beta = 0$, $\Gamma = 5$, $\eta = 1$, $|C_2|^2 = 0.1$, $|C_4|^2 = 1$, $|C_1|^2 = \epsilon|C_4|^2$, $|C_3|^2 = \epsilon|C_2|^2$, and $\epsilon = 10^{-9}$. Linear dependence of the numerical error on δz is evident.

threshold condition on the coupling strength $\Gamma_{\text{th}} = 2$ is obtained from Eq. (7).

Thus for DPC the transmissivity of the crystal in both directions is the same, $T_d = T_0 = T = \sin^2(u)$. We use this conclusion and the solution above to check our numerical procedure. As will be seen below, the equality of transmissivities does not hold in the transverse case, owing to the nonreciprocity of the scattering in PR crystals. It is interesting to note that by using the same method one can prove that DPC with reflection-type gratings $Q_R = A_1\bar{A}_3 + \bar{A}_2A_4$ is not possible. More precisely, DPCM with reflection-type gratings will not oscillate (however, it may amplify the finite beam seeds of C_1 and C_4).

3. INTEGRATION METHOD

The problem with the integration of Eqs. (1) and (4) lies in the nature of PR coupling and the split boundary conditions that have to be satisfied at the opposite faces of the crystal. We will attempt to accomplish integration within slight, but reasonable, approximations. The details of our algorithm are presented in Appendix C.

The spatial propagation problem of Eqs. (1) is addressed by a modified spectral BPM[13] used for mode calculations in bare or loaded unstable resonators. A solution of Eq. (4) is found by a Runge–Kutta or another initial-value algorithm. The procedure is facilitated by the fact that the temporal derivatives are neglected in Eqs. (1) and the spatial derivatives are neglected in Eq. (4). Thus the spatial integration can be separated from and nested within the temporal integration loop.

The thin gain sheets BPM could be applied directly to Eqs. (1) if the right-hand side of the jth beam equation were of the form $m(I)A_j$. However, this is not the case, and we modify the procedure to accommodate the new form, keeping the spirit of the BPM alive. We use the fact that the spatial equations are naturally paired into two sets, with two pairs of copropagating fields. Thus we concurrently propagate the pair (A_1, A_4) to the right and the pair (A_2, A_3) to the left, constantly modifying them for the coupling Q in an iterative self-consistent procedure. After the fields have converged into a quasi-stationary state corresponding to a given Q, the temporal evolution for a time step is performed.

Another problem is the geometry of beam coupling, with the two counterpropagating pairs of beams contributing to Q. As the source of coupling in the spatial domain is the grating amplitude Q (proportional to the space-charge field in the crystal), it must be known at each instant of time at all locations in the crystal. Likewise for the total intensity I, which figures explicitly in Eq. (4) (and is not an integration constant in the time-dependent transverse case). This makes stringent requirements on the computer core space.

In the PW case ($\beta = \phi = 0$) we find good agreement between the numerical and the analytical solutions (Fig. 3). If transverse effects are included and Gaussian input beams are used, the intensities of the PC beams (I_1, I_3) decrease compared with those in the PW case. The inclusion of diffraction is always detrimental to the process of DPC. Likewise, the inclusion of absorption is also detrimental to the process of DPC.

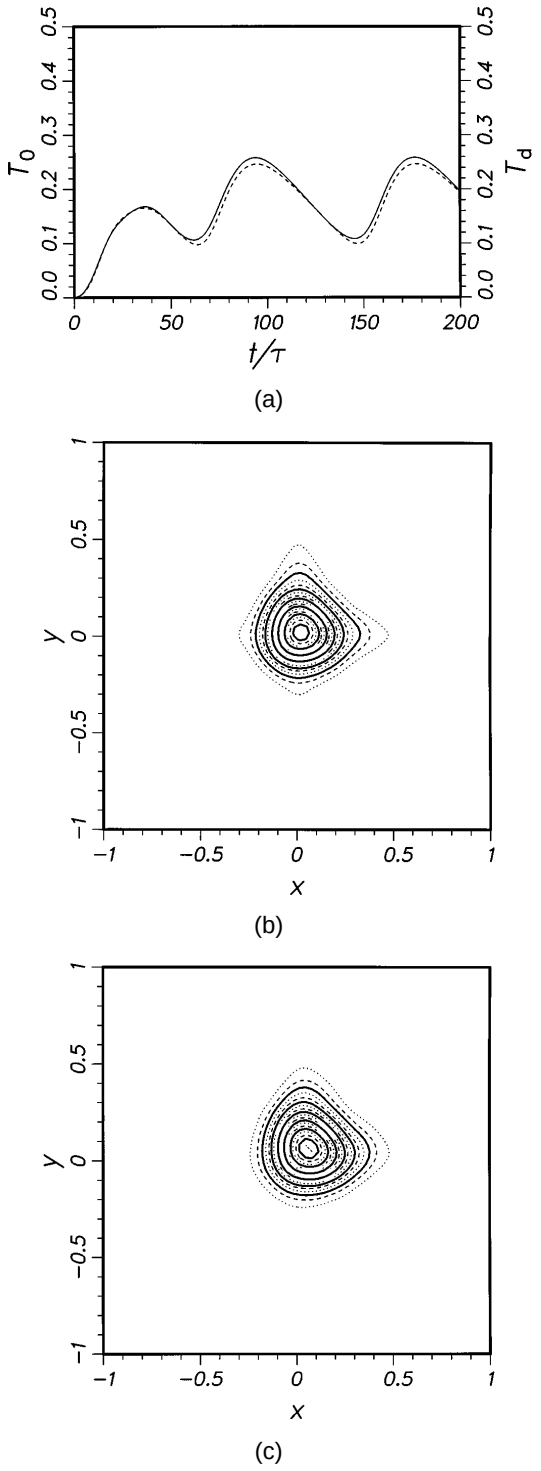

Fig. 4. (a) Limit cycle oscillation of the total transmissivity. Solid curve, T_0; dashed curve, T_d. (b) Contour plot of the output profile I_3 versus transverse coordinates at $t = 150\tau$. The profile is shifted from the center at $x = 0$, $y = 0$ in the direction $y = x$ of the grating wave vector. (c) The profile at $t = 180\tau$, close to the maximum of the cycle. The parameters are as in Fig. 3, except that $\Gamma = 3$, $\epsilon = 10^{-5}$, and the nonzero $\phi = 0.01$.

4. SPATIAL EFFECTS

A. Self-Bending

The inclusion of transverse dimensions produces an interesting readily observable effect: self-bending of PC beams. This is a genuine transverse effect, caused (and

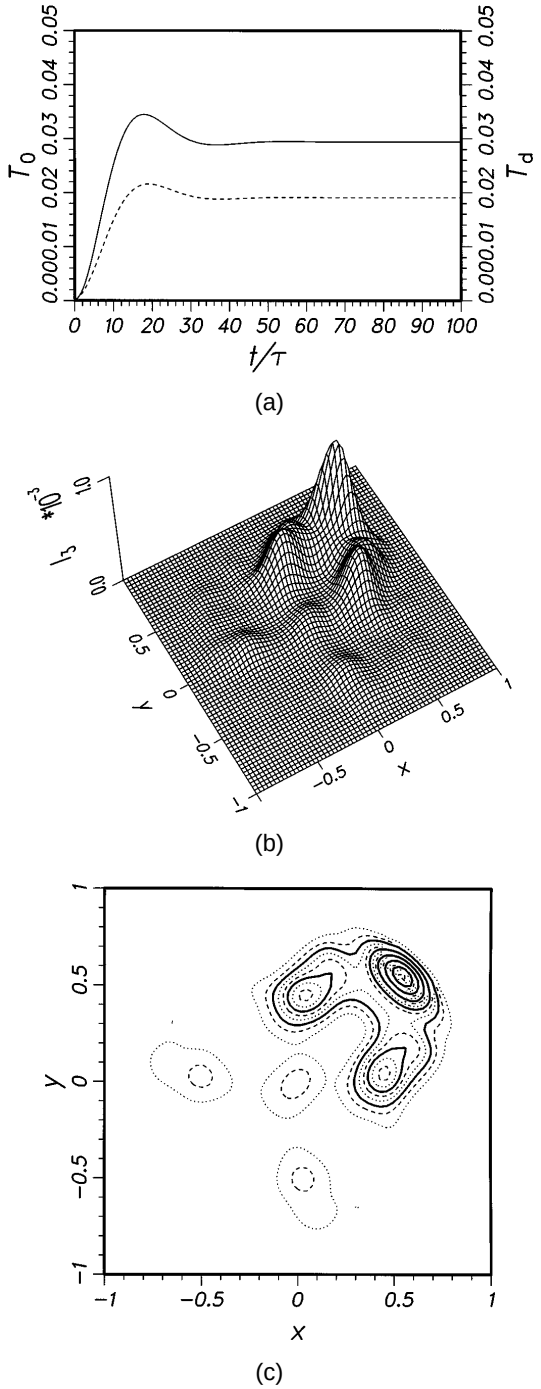

Fig. 5. (a) Total transmissivities in the steady-convection state when numerical absorption is introduced at the edge of the crystal. The parameters are as in Fig. 4, except for the higher value of ϕ ($\phi = 0.03$). (b) Transverse profile of I_3. (c) Transverse profile of I_3 represented as a contour plot, displaying the $y \leftrightarrow x$ symmetry built into the model. This symmetry fixes the direction of convection.

controlled) by the finite beam waist and not by the (possible) phase mismatch. It appears even in the diffractionless case ($\phi = 0$), provided that convective effects ($\beta \neq 0$) are taken into account.[3] The physical origin of self-bending is the convective flow of energy out of the interaction region.[3,15] The inclusion of diffraction leads to more-complicated transverse patterns and causes the degradation of PC beam quality. In this section we present some numerical calculations in which we use the above-mentioned Gaussian input beams, with $\xi = 0$ and $\sigma = 0.2$. The amplitudes C_1 and C_3 are kept very small. However, they cannot be set to zero because the process needs some (noisy) seed to start up. In addition to Gaussians we tried true noisy inputs (using random-number generators) and obtained the same results.

Figure 4(a) shows the temporal evolution of the total transmissivity (integrated over the transverse dimen-

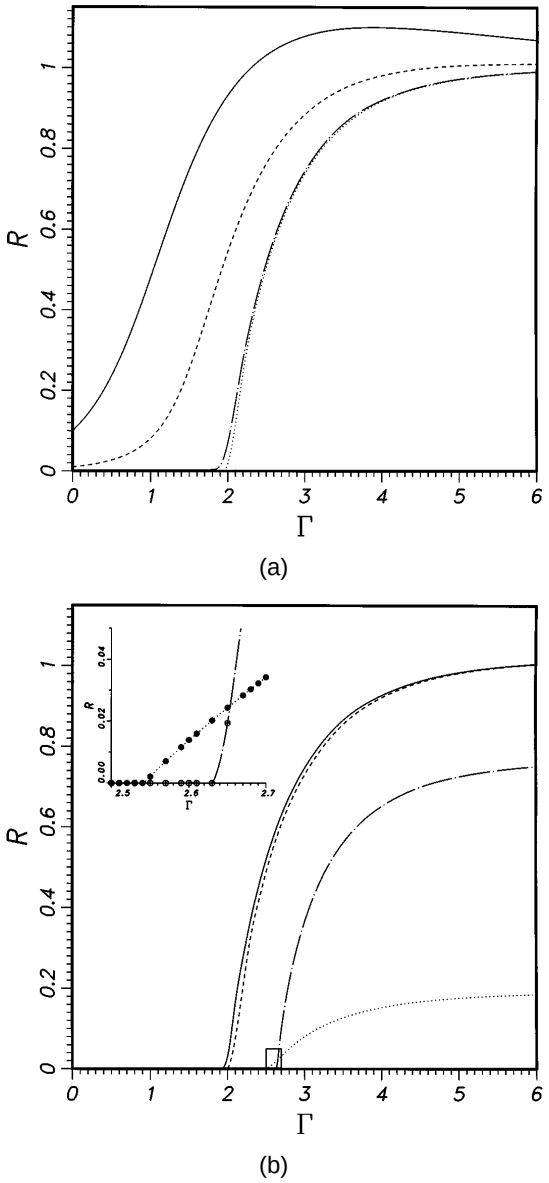

Fig. 6. Reflectivities $R = R_0 = R_d$ as functions of the coupling strength Γ for $\beta = 0$. The amplitudes of the Gaussian pump beams are chosen equal, $C_2 = C_4 = 1$, whereas the input of PC beams $|C_1|^2 = |C_3|^2 = \epsilon$ is varied. (a) PW results for different beam seeds ϵ: solid curve, $\epsilon = 10^{-1}$; dashed curve, $\epsilon = 10^{-2}$; dotted–dashed curve, $\epsilon = 10^{-5}$; dotted curve, $\epsilon = 10^{-9}$. The reflectivities are calculated by both the analytical formulas and the numerical method (with $\phi = 10^{-20}$). The threshold condition $\Gamma_{\text{th}} = 2$ for oscillation is clearly visible. (b) Reflectivities in the transverse case for different ϕ and the fixed seed ($\epsilon = 10^{-9}$): $\phi = 10^{-20}$ (solid curve), $\phi = 10^{-2}$ (dashed curve), $\phi = 10^{-1}$ (dotted–dashed curve), $\phi = 1$ (dotted curve). The inset shows an enlargement of the take-off region for $\phi = 0.1$ and $\phi = 1$. The threshold is now smeared over an interval, and for higher ϕ it might even not exist.

sions) at both faces of the crystal. In the transverse case $T_0 \neq T_d$. However, the analytical PW formulas $R_0 = T_0/r$ and $R_d = rT_d$ (where r is the ratio of input intensities, $r = |C_4/C_2|^2$) are still valid. Figures 4(b) and 4(c) depict the tilt of the beam I_3 away from the center $x = 0$, $y = 0$ of the transverse plane at $z = 0$. The transverse distribution of the beam represents a breathing-deformed Gaussian mode. Breathing in this context means a periodic change of the transverse intensity pattern from a minimum to a maximum. The performed Gaussian mode is symmetric with respect to the $y = x$ axis. It keeps the prescribed symmetry in force. We assume that in this case the regular shift is caused by nonequal values for the input seeds of the PC beams.

If the influence of diffraction in increased (higher values of ϕ), a state of steady convection is reached, with further spatial widening of the PC beam and the appearance of local maxima in the beam profile (Fig. 5). The drift of the output profile away from the center is more pronounced, but eventually it is controlled by the physical size of the crystal or by some other nonlinear loss mechanism. In the simulations we damp the fields at the edge of the numerical grid. The drift of interacting fields in the crystal (or the domains of interaction) to the side of incident pumps is observed experimentally.[4,16]

Our results agree with the recent research on two-dimensional DPCM's[3] only when directional effects are included and diffraction excluded, and even then only qualitatively. We conclude that a DPCM with diffraction is a convective oscillator. However, for strong diffraction and strong couplings more-complicated spatiotemporal phenomena are observed. The reasons for the discrepancy are probably that the theory in Ref. 3 is linear (it applies to low-reflectivity levels), in the numerical results diffraction is neglected, and the theory is derived for a rather special two-dimensional geometry. It does not contain transverse Laplacian.

B. Oscillation versus Amplification

The convective flow of energy helps to resolve the controversy between oscillation and amplification. The authors of Ref. 3 believe that the transport of energy is the mechanism for inhibition of oscillation. In the PW case such a mechanism is absent.

We believe that, in addition to convection, an important mechanism is the multimode operation of DPCM when transverse dimensions are accounted for. The Fresnel number F determines the maximum number of transverse modes that can oscillate.[17] In general, the number of possible transverse modes scales as F^2. Which transverse modes oscillate depends on the boundary conditions, coupling strength, and other details of the experimental setup. Different spatial modes have different oscillation thresholds. In the transverse case there is no precise threshold condition for oscillation. When more than one mode can oscillate, the oscillation does not start at a particular value of coupling but is turned on gradually over an interval. A more realistic transverse model changes the sharp steplike transition at the threshold into a more gradual continuous transition, with finite (though large) derivatives. This is clearly visible in Fig. 6, which depicts the amplification of different beam seeds for the same value of ϕ ($\phi = 10^{-20}$) and the amplification of the same seed ($|C_1|^2 = |C_3|^2 = \epsilon = 10^{-9}$) for different ϕ. The interval of threshold conditions is seen in Fig. 6(b).

Figure 7 represents the amplification of different seeds for different values of ϕ on the logarithmic scale. The shift toward larger couplings and a less steep rise is visible. Figures 6 and 7 are obtained for $\beta = 0$. In general, $\beta = 0$ does not mean that the beams are actually collinear. It means that the ratio of the angle at the beams' intersection to the angular spread of the beams is small and hence neglected. The figures also display how subtle these effects are when investigated numerically. Qualitatively, different cases look similar. However, the existence of an oscillation threshold is evident in all the cases. As the threshold is approached, critical slowing down is observed. For small ϵ it takes long times to achieve convergence. Below threshold the device acts as an amplifier; above threshold it is an oscillator. Also, the appearance of convection is evident when transverse dimensions are accounted for. Having to choose between a convective amplifier and an optical oscillator in describing a DPCM, we believe that the appropriate choice is a convective oscillator.

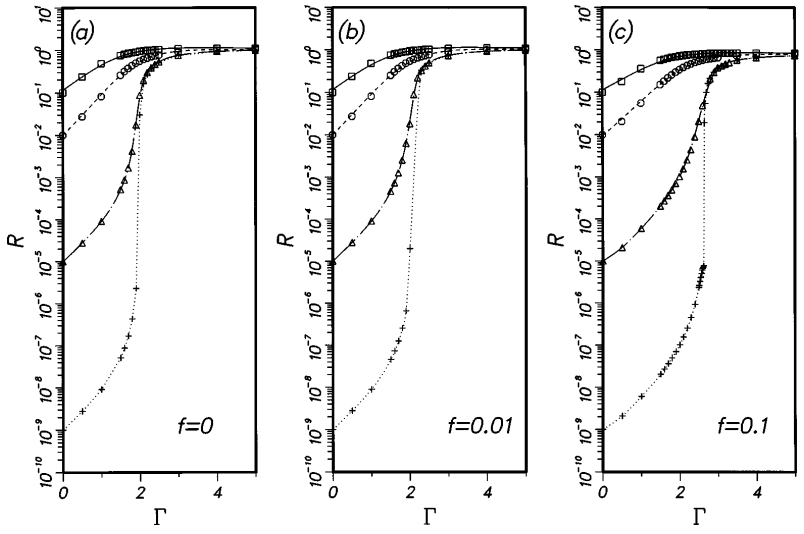

Fig. 7. Reflectivities versus coupling strength on the logarithmic scale for different seeds ϵ. The existence of an oscillation threshold as ϵ goes to zero is evident. Below the threshold DPCM is an amplifier; above the threshold the saturation of reflectivities is noted. The shift of the threshold and the reduction of derivatives are shown for three values of $\phi = f$: squares, $\epsilon = 10^{-1}$; circles, $\epsilon = 10^{-2}$; triangles, $\epsilon = 10^{-5}$; crosses, $\epsilon = 10^{-9}$. The curves are polynomial fits through the points, drawn to guide the eye.

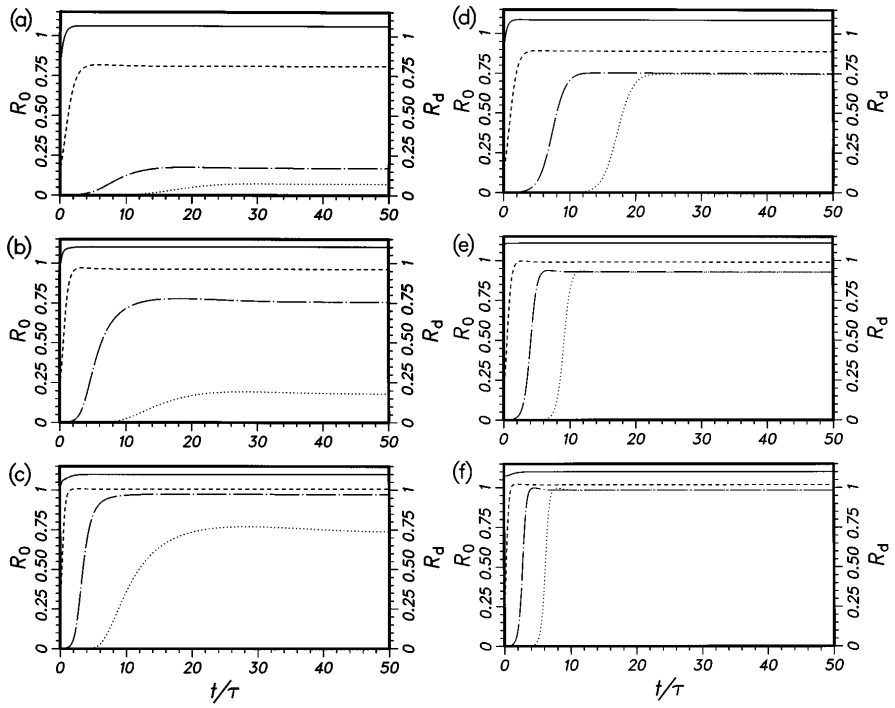

Fig. 8. Dynamics of the oscillation switch on, for two values of the transverse displacement β and for different values of the coupling strength Γ. Total reflectivities are presented as functions of time for different values of the seed ϵ (solid curves, $\epsilon = 10^{-1}$; dashed curves, $\epsilon = 10^{-2}$; dotted–dashed curves, $\epsilon = 10^{-5}$; dotted curves, $\epsilon = 10^{-9}$). For (a)–(c) $\beta = 0.1$, and the device acts as an amplifier. For (d)–(f) $\beta = 0.01$, and the device acts as an oscillator. In (a) (when the whole curve for $\epsilon = 10^{-9}$ is multiplied by 50) and (d) $\Gamma = 3$, in (b) and (e) $\Gamma = 4$, and in (c) and (f) $\Gamma = 5$. Here $\phi = 0$.

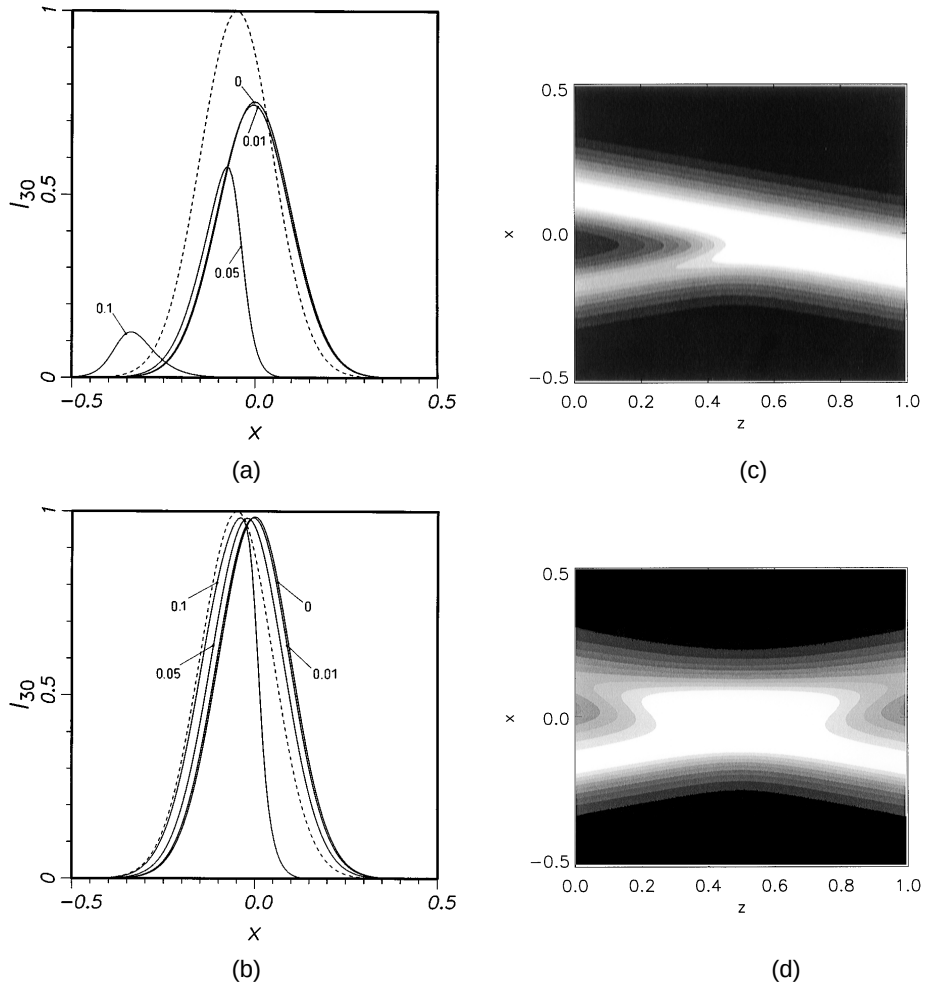

Fig. 9. Transverse profiles of the beam I_{30} for $\phi = 0$ and $\epsilon = 10^{-5}$ and for different values of the coupling strength Γ and of the transverse displacement β: (a) $\Gamma = 3$, (b) $\Gamma = 5$. The value of β is given in each figure. The dashed curves are profiles of one of the pumps (for $\beta = 0.1$). (c) Spatial transverse distribution of beams I_2 and I_3 in the crystal for $\beta = 0.2$ and $\Gamma = 5$. A small amount of seed ($\epsilon = 10^{-5}$) and of diffraction ($\phi = 2.72 \times 10^{-4}$) is included. (d) Same as (c) for the total intensity.

An emerging physical picture concerning amplification and oscillation is as follows. For $\phi = 0$ and $\beta = 0$ the DPCM is an oscillator. For $\phi \neq 0$ and $\beta = 0$ it is a convective oscillator. For $\phi = 0$ and $\beta \neq 0$ it is an oscillator up to a critical transverse displacement β_c. Above β_c it is a convective amplifier.[3] For $\phi \neq 0$ and $\beta \neq 0$ the situation is not so clear. There seems to exist a critical curve in the (β, ϕ) plane below which the device acts as a convective oscillator and above which it acts as a convective amplifier. Owing to critical slowing down, the investigation of such a critical curve is computationally expensive.

Figure 8 shows the influence of β for $\phi = 0$. Two values of β are chosen, one well below the critical value β_c and the other well above the critical value. The value of the critical transverse displacement depends on the coupling strength. Figure 9 presents transverse profiles of the PC beam I_{30} for different values of the coupling strength and of the transverse displacement. Also represented is the transverse distribution of beams in the crystal during the DPC process [Figs. 9(c) and 9(d)].

C. Transverse Patterns

The inclusion of transverse dimensions leads to rich spatial and temporal phenomena.[10,17] Here we present

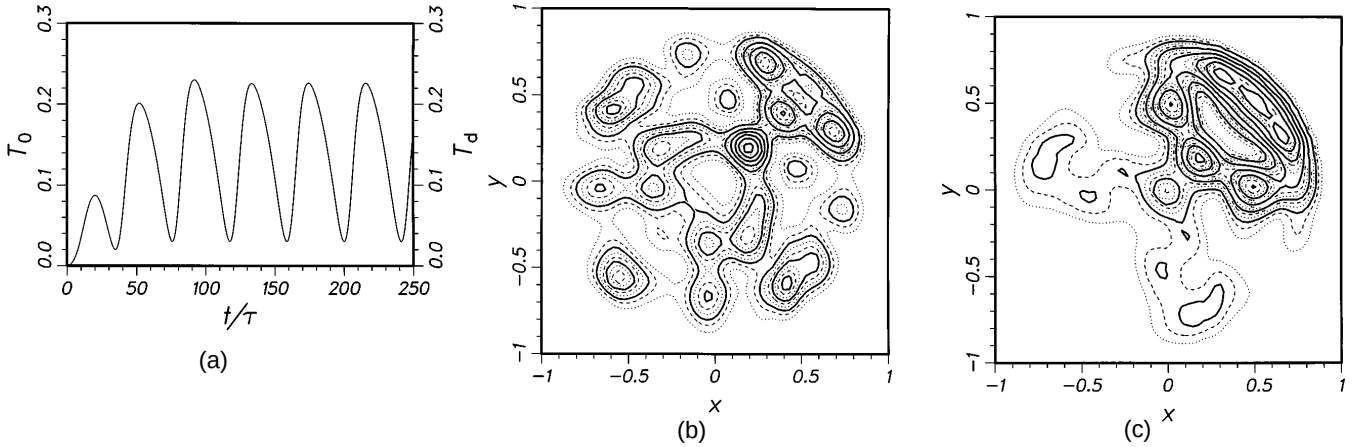

Fig. 10. (a) Dynamics of the total transmissivities $T = T_0 = T_d$ for $\phi = 0.05$ and $\Gamma = 3$. (b) Contour plot of the transverse profile of I_3 close to the cycle minimum at $t = 215\tau$. (c) Contour plot at the cycle maximum, $t = 240\tau$.

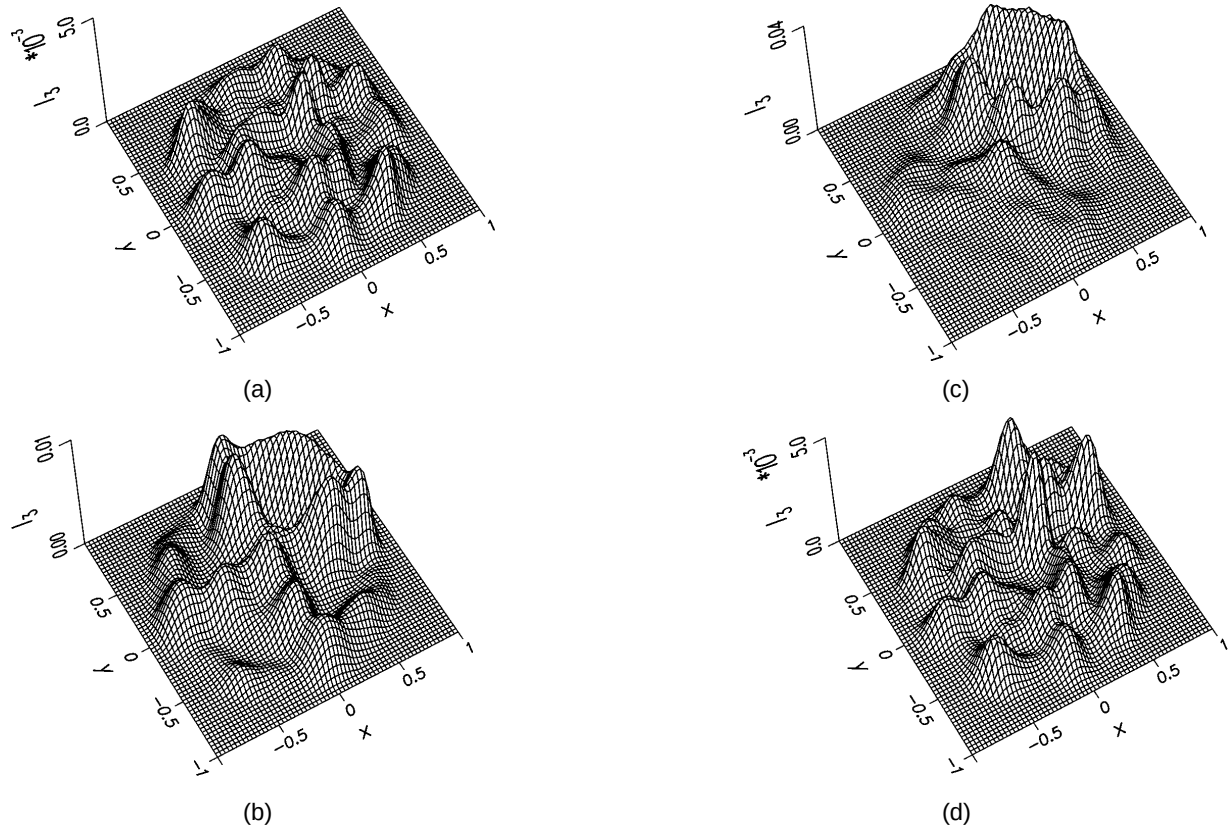

Fig. 11. Transverse patterns of the PC field I_3 at four locations during one cycle in Fig. 10. (a) $t = 200\tau$, (b) $t = 205\tau$, (c) $t = 215\tau$, (d) $t = 240\tau$. A periodic rise of the convective pulse is observed. The pulse is absorbed at the edge of the crystal.

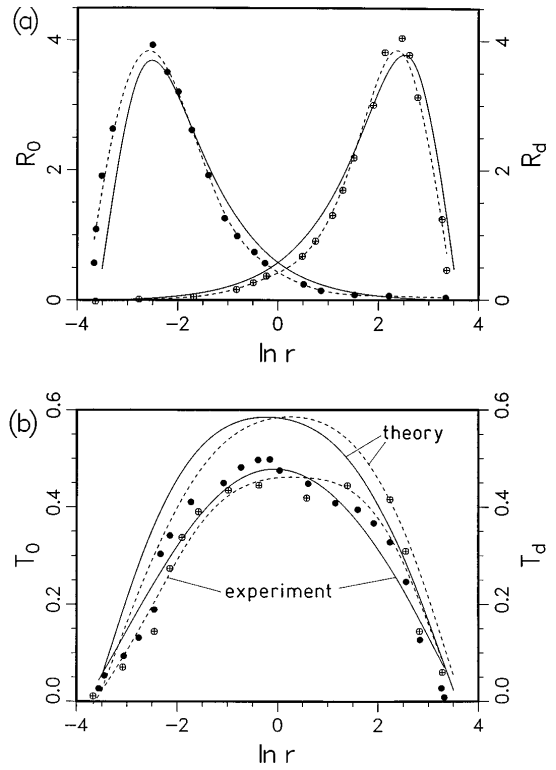

Fig. 12. Comparison with the experimental results of Ref. 2: (a) Reflectivities R_0 and R_d at both sides of the crystal as functions of the pump ratio r. Filled circles are the experimental values of R_0, and crossed circles are the values of R_d. Dashed curves are polynomial fits through the experimental points. Solid curves are numerical curves with $\Gamma = 4$ and $\phi = 0.121$. (b) Corresponding transmissivities T_0 and T_d. One of the solid curves is a fourth-order polynomial fit through the experimental points for T_0, and the other is the corresponding numerical curve. Dashed curves are the same for T_d.

a periodic solution (limit cycle) with a more-complicated transverse structure. A limit cycle is a periodic solution that sets up after one Hopf bifurcation in the system. In this context it is a solution with constant intensity of any beam and with the phases circling clockwise or counterclockwise in time. It is difficult to speak of phase conjugation now, because the output profile I_3 bears little resemblance to the input profile I_4. The difference from the previous example of convection (Fig. 5) lies in the higher value of the ϕ parameter and in the equal input pumps ($C_2 = C_4 = 1$). However, the Fresnel number is still large enough to permit the excitation of more than one spatial mode. Figure 10 shows the temporal evolution of the total transmissivity T and the contour plots of the transverse beam profiles at approximately the minimum and the maximum of the limit cycle oscillation. Figure 11 depicts consecutive snapshots of the transverse profiles at four instants during one cycle. The dynamics of the cycle proceeds from a weak but complicated profile at the minimum to a strong convective pulse at the maximum. The pulse gets absorbed at the grid edge, with the consequent loss of energy, and the cycle repeats. Such behavior is characteristic of a spatially and temporally ordered state. We did not observe chaos, neither temporal nor spatiotemporal, as long as the coupling constant remained real. This agrees with the conclusions of an earlier report[11] on chaos in single-grating single-interaction-region 4WM. However, that report is concerned with a PW model.

D. Comparison with Experiment

The inclusion of transverse effects improves the agreement between numerical and experimental results. The theory based on PW analysis consistently gives too high estimates for the intensity reflectivity.[2] Figure 12 offers a comparison between numerical and experimental results. The only fitting parameter here is the value of ϕ. For $\phi = 0.121$ a good agreement for R_0 and R_d is found. A more improved agreement could easily be obtained by inclusion of linear absorption and/or noncollinearity. However, we prefer the figure as is, as it clearly displays another tiny but important transverse effect: nonreciprocity. That is, the transmissivities at the 0 face and at the d face of the crystal in the transverse case are not equal because the scattering off PR gratings is nonreciprocal.

5. DYNAMICAL EFFECTS

Analysis of stable patterns that can set up in PR oscillators is the first step in an investigation of spatiotemporal instabilities and the road to chaos through the generation and dynamics of structural defects.[10,17]

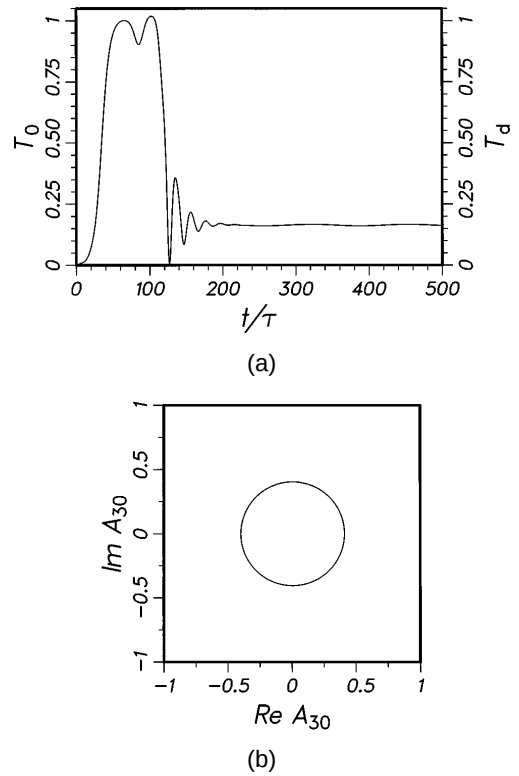

Fig. 13. Temporal signal for an ordered PW state with the external electric field applied transversely across the crystal (along the x direction). (a) Transmissivities, (b) phase portrait of the lower, stable state, showing that indeed it is a limit cycle. The parameters are $|C_1|^2 = |C_3|^2 = 10^{-5}$, $|C_2|^2 = |C_4|^2 = 1$, $\Gamma_0 = 4$, $\phi = 10^{-20}$, $E_M = 100$, $E_q = 5$, $E_D = 1$, and $E_0 = 4$ (arbitrary units).

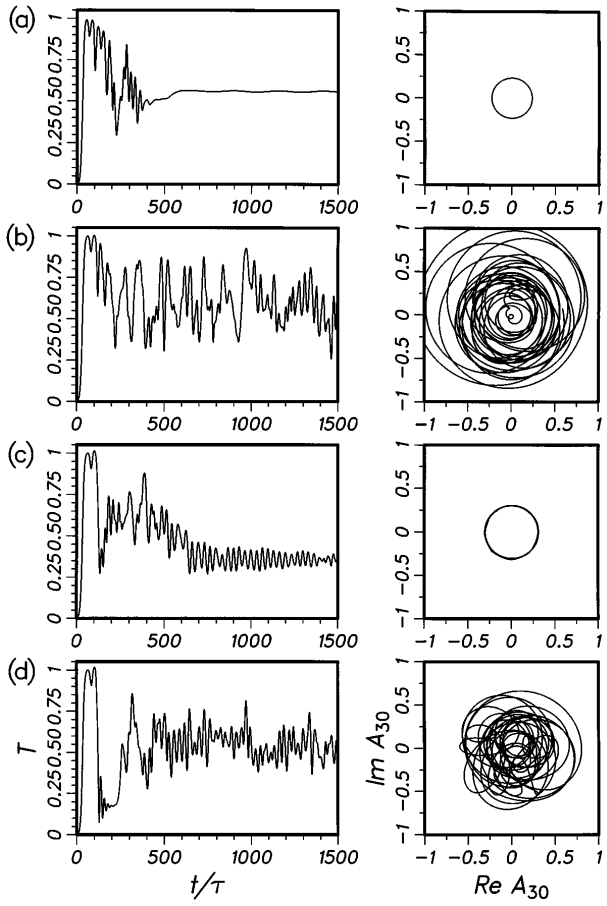

Fig. 14. Temporal behavior with the inclusion of transverse effects. Left column, transmissivity $T = T_0 = T_d$; right column, phase portrait of A_3 (at $z = 0$) in the center of the beam after 1000τ steps. The same parameters as in Fig. 13, except for (a) $\phi = 0.006$, (b) $\phi = 0.003$, (c) $\phi = 0.002$, (d) $\phi = 0.001$.

We would like to know under what conditions chaotic or turbulent dynamics can arise in our model. As mentioned, the inclusion of transverse effects does not change one of the key conclusions of our previous analysis: the lack of chaos for real couplings. Realistic spatiotemporal complexity can be introduced in two ways: by applying an external electric field E_0 across the crystal[11] and/or by introducing phase mismatch in the wave interaction.

The first method makes the couplings between the waves complex,

$$\Gamma = \Gamma_0 \frac{E_q + E_D}{E_D} \frac{E_D + iE_0}{E_M + E_D + iE_0}, \tag{8a}$$

$$\eta = \frac{E_D + E_q + iE_0}{E_M + E_D + iE_0}, \tag{8b}$$

and promotes multimode competition in the crystal[18] owing to the presence of external electric field E_0; the other violates the Bragg condition and introduces competition between the grating-writing interference terms $A_1\overline{A}_4$ and $\overline{A}_2A_3$. Here we investigate only the first method. We further restrict ourselves to an example in which chaotic behavior is introduced exclusively by the transverse spread of beams. For the characteristic internal electric fields of the PR crystal E_D, E_M, and E_q we use the values consistent with the data obtained for barium titanate. We also set $\beta = 0$.

The dynamics of the starting PW state is presented in Fig. 13. The system starts to oscillate in the fundamental high-reflectivity mode, which however turns out to be unstable for this high value of the electric field E_0. The instability grows until the system switches to a stable low-reflectivity mode.

The situation changes dramatically with the inclusion of transverse dimensions. Figure 14 shows the temporal evolution of the transmissivity T and the phase portraits of A_3 for different values of the diffraction coupling ϕ. T settles onto a fixed value only for large ϕ [Fig. 14(a)]. This state becomes unstable for smaller ϕ and oscillates irregularly [Fig. 14(b)]. The decreasing values of ϕ correspond to the increasing values of the Fresnel number. A stationary oscillation is found [Fig. 14(c)], and the final state represents another chaotic attractor [Fig. 14(d)].

The overall spatiotemporal behavior of these states is represented in Fig. 15. The stationary state is formed by a beam profile with two local maxima [Fig. 15(a)]. On reduction of ϕ the left peak is suppressed, and the intensity oscillates irregularly in space and time around the right peak [Fig. 15(b)]. On further reduction in ϕ a periodic

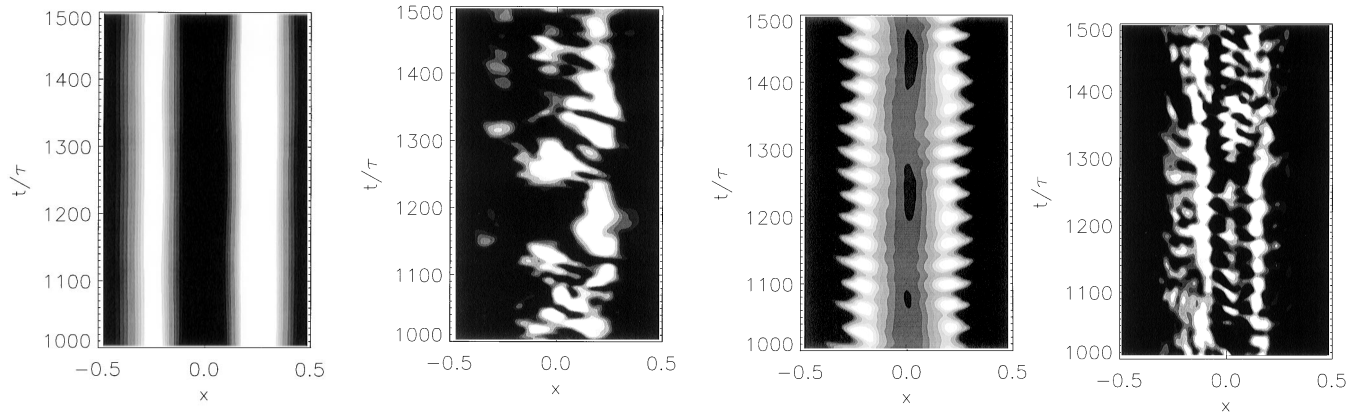

Fig. 15. Temporal transverse signal of the field $I_3(x)$ after the transients have died away. The parameters are as in Fig. 14.

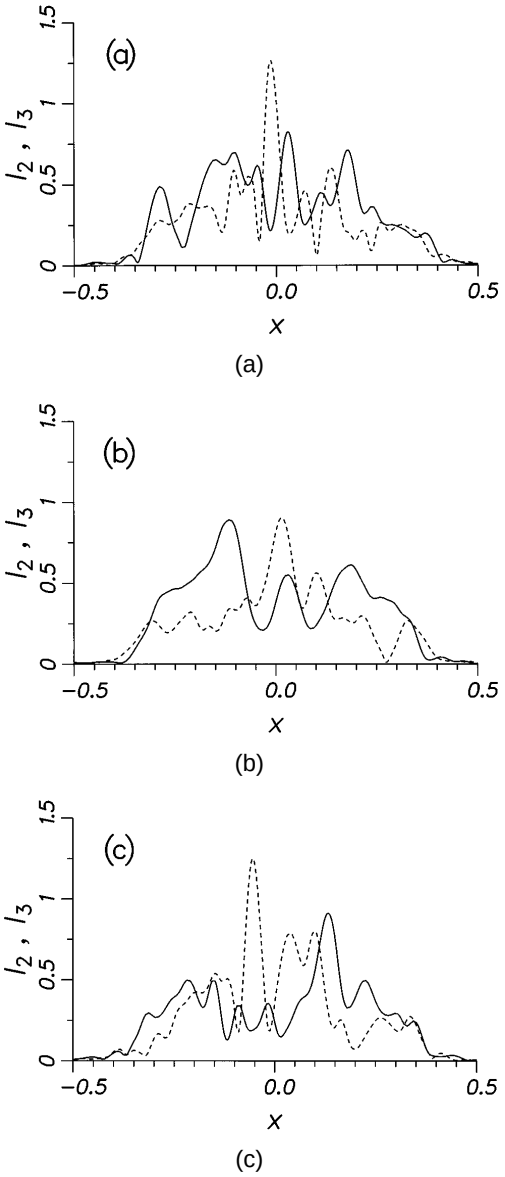

Fig. 16. Filamented transverse profiles of I_3 (solid curves) and I_2 (dashed curves) at $z = 0$ at different instants: (a) $t = 1000\tau$, (b) $t = 1300\tau$, (c) $t = 1500\tau$. The simulation corresponds to that of Figs. 14(d) and 15(d). Note the partial anticorrelation between the I_3 and the I_2 peaks.

spatiotemporal state is reached [Fig. 15(c)], where two intensity peaks oscillate coherently to each other. This coherence is lost in Fig. 15(d), and a final state of spatiotemporal chaos is formed in which the dynamics of different spatial signals is different. Whereas some vague transverse spatial correlation of the signal is visible, temporally the signal at any spatial location is chaotic. The spatial correlation length is reduced in going from the state in Fig. 15(b) to the state in Fig. 15(d).

Owing to strong diffraction effects the filamentation of transverse output profiles is noticeable (cf. Fig. 16). The filamentation of PC beam A_3 occurs as a result of suppression of pump beam A_2, which by means of the complex PR coupling Γ introduces a self-focusing nonlinearity into the wave equations. This effect is clearly visible if one looks at the intensity I_3 in the crystal, as shown in Fig. 17. Different peaks with high intensities occur and focus during the propagation through the crystal. The filamentation of beams becomes stronger for smaller values of the coupling ϕ (not shown here). Depending on the values of other parameters, the filaments move transversely or from standing patterns. With an increased electric field, a complicated dynamics of traveling transverse waves arises. This is consistent with the expectation that more-complex diffraction phenomena should occur for higher (but finite) values of the Fresnel number. The system displays an interesting example of transition

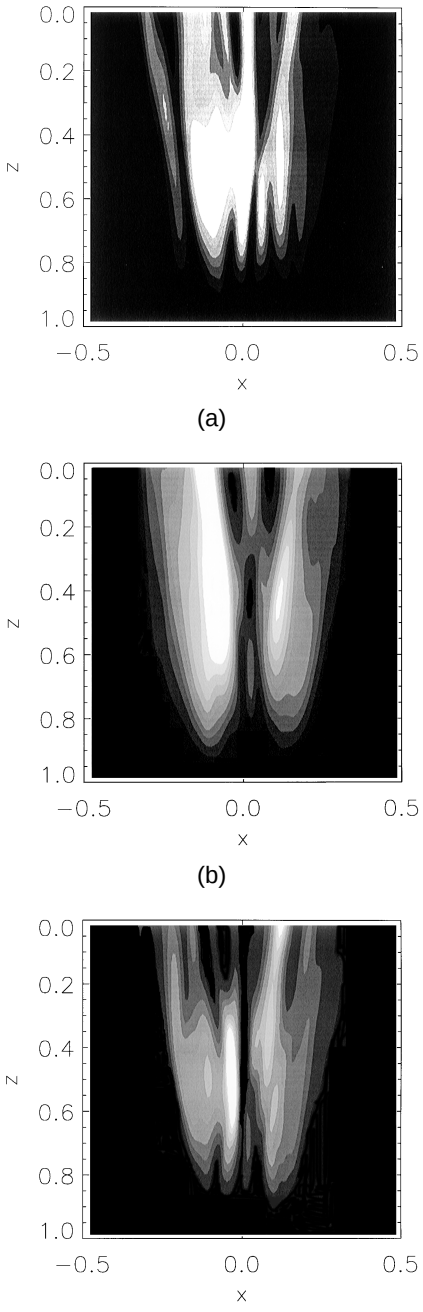

Fig. 17. Transverse distribution of the field I_3 in the crystal at different times. (a) $t = 1000\tau$, (b) $t = 1300\tau$, (c) $t = 1500\tau$. The simulation corresponds to that of Figs. 14(d) and 15(d).

to spatiotemporal chaos through mode competition, and we are in the process of quantifying it.

6. CONCLUSIONS

In summary, we have studied transverse and dynamical effects in the DPCM. We find that the inclusion of the finite lateral beam extension lowers the reflectivities, bends the beams, and resolves the controversy about the nature of DPC. It also improves the agreement with experimental results and accounts for the experimentally observed asymmetry between the transmissivities of the crystal along the beam incidence.

In numerical simulations one always needs a finite seed for the process of start up; however, one can obtain useful information from the way in which the system behaves as the seed is getting smaller. Based on such an information (and confirmed by theoretical results from Section 2), we conclude that in the PW approximation the DPCM is an oscillator with the gain threshold ($\Gamma_{\text{th}} = 2$ for equal pumps). Exponential growth of PC beams is observed above the threshold for arbitrarily small seeds. Seeds are needed only as an initial push. Reflectivity levels attained do not depend on the seed, with marked saturation owing to the depletion of pumps. Below threshold the reflectivity depends directly on the seed, going to zero as the seed is diminished.

In our transverse model the DPCM is a convective oscillator rather than an amplifier. The gain threshold is not well defined. However, the existence of an oscillation threshold for each value of the diffraction parameter ϕ is evident. Again, below the threshold region the device acts as an amplifier; different seeds are amplified to different levels. Above the threshold the reflectivities depend little on the seed, and the signal persists even in the absence of the seed. When the influence of transverse displacement is included, for low values of β the device is an oscillator up to a critical value β_c. Above the critical value of the transverse displacement the device becomes a convective amplifier.

With the inclusion of transverse dimensions the intensity distributions of PC beams become shifted and asymmetric. The bending of beams is caused by the convective flow of energy. Steady convection is observed numerically and is also evident in the experiment.[4,16] Also, the convergence of the transverse model is faster than that of the PW model of 4WM.

For strong (real) couplings instabilities are noted, in that the reflectivity (and transmissivity) does not settle onto any fixed value but oscillates regularly. However, in this case the output profile is complicated, and it is difficult to speak of phase conjugation.

A rich dynamical behavior including spatiotemporal chaos is observed when a dc electric field is applied across the crystal. This makes the PR coupling complex. Then the self-focusing that is due to the nonlinearity is in competition with the diffraction in the crystal. All these effects act destructively toward the process of phase conjugation. We observe competition between different spatial modes, traveling transverse waves, and defect-mediated turbulence in our system. Such spatiotemporal instabilities are under current investigation.

APPENDIX A: DERIVATION OF PARAXIAL WAVE EQUATIONS FOR DOUBLE PHASE CONJUGATION

We start by writing paraxial wave equations for each of the two propagation arms:

$$\partial_{z''} A_1 + \frac{i}{2k} \Delta_T'' A_1 = Q A_4 , \tag{A1a}$$

$$\partial_{z''} A_2 - \frac{i}{2k} \Delta_T'' A_2 = \overline{Q} A_3 , \tag{A1b}$$

$$\partial_{z'} A_3 - \frac{i}{2k} \Delta_T' A_3 = -Q A_2 , \tag{A1c}$$

$$\partial_{z'} A_4 + \frac{i}{2k} \Delta_T' A_4 = -\overline{Q} A_1 , \tag{A1d}$$

where the directions of the wave vectors $\mathbf{k}_4$ and $\mathbf{k}_1$ define the z' and z'' axes and Δ_T' and Δ_T'' are the corresponding transverse Laplacians. We use the same set of symbols $\{A_j, Q\}$ to denote the fields and the grating amplitude in all the cases. For the moment we consider only one transverse dimension and assume that the angle between the propagation arms is small. The equation $k = 2\pi n_0/\lambda$ denotes the magnitude of wave vector $|\mathbf{k}_j|$ in the medium. A degenerate situation is assumed. One then makes a transformation to the common set of (x, z) coordinates, where the z axis points halfway between z' and z''. Equations (A1) become

$$\partial_z A_1 + \theta \partial_x A_1 + \frac{i}{2k} (\partial_x{}^2 - 2\theta \partial_x \partial_z) A_1 = Q A_4 , \tag{A2a}$$

$$\partial_z A_2 + \theta \partial_x A_2 - \frac{i}{2k} (\partial_x{}^2 - 2\theta \partial_x \partial_z) A_2 = \overline{Q} A_3 , \tag{A2b}$$

$$\partial_z A_3 - \theta \partial_x A_3 - \frac{i}{2k} (\partial_x{}^2 + 2\theta \partial_x \partial_z) A_3 = -Q A_2 , \tag{A2c}$$

$$\partial_z A_4 - \theta \partial_x A_4 + \frac{i}{2k} (\partial_x{}^2 + 2\theta \partial_x \partial_z) A_4 = -\overline{Q} A_1 , \tag{A2d}$$

where θ is the (small) half-angle between the incident beams. Next, the equations are made dimensionless by introduction of the characteristic longitudinal length (the crystal thickness d) and the characteristic transverse length (the beam spot size ω_0). One obtains

$$\partial_z A_1 + \frac{\theta}{\delta} \partial_x A_1 + i\phi (\partial_x{}^2 - 2\theta\delta \partial_x \partial_z) A_1 = Q A_4 , \tag{A3a}$$

$$\partial_z A_2 + \frac{\theta}{\delta} \partial_x A_2 - i\phi (\partial_x{}^2 - 2\theta\delta \partial_x \partial_z) A_2 = \overline{Q} A_3 , \tag{A3b}$$

$$\partial_z A_3 - \frac{\theta}{\delta} \partial_x A_3 - i\phi (\partial_x{}^2 + 2\theta\delta \partial_x \partial_z) A_3 = -Q A_2 , \tag{A3c}$$

$$\partial_z A_4 - \frac{\theta}{\delta} \partial_x A_4 + i\phi (\partial_x{}^2 + 2\theta\delta \partial_x \partial_z) A_4 = -\overline{Q} A_1 , \tag{A3d}$$

where $\delta = \omega_0/d$ is the beam's angular spread and $\phi = (4\pi F)^{-1}$ is related to the Fresnel number $F = \omega_0{}^2/\lambda d$. Now z and x are dimensionless numerical variables confined to an appropriately chosen computational domain. Normally θ, δ, and ϕ are small, so that the mixed derivative correction to the transverse Laplacian can be neglected. However, the convective term involving $\partial_x A_j$

cannot be neglected because the quantity $\beta = \theta/\delta$ need not be small.

The extension to two transverse dimensions is easy. Assuming that the wave vector of the grating $\hat{K}$ (lying in the transverse plane) makes an angle ψ with the x axis, the directional derivative becomes $\hat{K} \cdot \nabla_T = \cos(\psi)\partial_x + \sin(\psi)\partial_y$. We pick $\psi = \pi/4$ and absorb the $\sqrt{2}$ factor into the β. Likewise the transverse Laplacian becomes $\partial_x{}^2 + \partial_y{}^2$.

One should note that the electric fields formed by use of slowly varying envelopes carry additional phases of the form $\exp(ikz')$ and $\exp(ikz'')$. On transformation and scaling of the coordinates, the optical phase of various beams acquires the form $kd(z \pm \theta\delta x)$. This phase takes into account the noncollinear propagation of two pairs of beams. In the spirit of paraxial approximation the second term in the optical phase can be neglected. However, when instabilities and traveling transverse waves are discussed, the second term must be included in the analysis.

APPENDIX B: PLANE-WAVE SOLUTION OF FOUR-WAVE MIXING EQUATIONS

In the steady state, the expression for Q (with $\eta = 1$) from Eq. (4) is included in Eqs. (1), with $\beta = 0$ and $\phi = 0$, and the resulting equations are solved as a system of first-order ordinary differential equations. The details of the solution are provided in Ref. 14.

For Γ real the system of Eqs. (1) is linearized with the following transformation of the independent variable:

$$\Theta' = \frac{\Gamma|Q|}{I}, \tag{B1}$$

where the prime denotes the derivative along the propagation direction z. The solution is then given by

$$A_1 = C_1 \cos(\Theta - \Theta_0) + C_4 \sin(\Theta - \Theta_0), \tag{B2a}$$

$$A_4 = C_4 \cos(\Theta - \Theta_0) - C_1 \sin(\Theta - \Theta_0), \tag{B2b}$$

$$A_3 = C_3 \cos(\Theta_d - \Theta) + C_2 \sin(\Theta_d - \Theta), \tag{B2c}$$

$$A_2 = C_2 \cos(\Theta_d - \Theta) - C_3 \sin(\Theta_d - \Theta), \tag{B2d}$$

where $C_{1\text{-}4}$ are the given boundary values of the four fields: $A_{1,4}(z = 0) = C_{1,4}$ and $A_{2,3}(z = d) = C_{2,3}$. Using this solution, one finds an expression for the grating amplitude:

$$2|Q| = aI \sin(2\Theta), \tag{B3}$$

where a is a constant to be determined from the boundary conditions. For a transmission grating process the total intensity I is also constant, $I = |C_1|^2 + |C_2|^2 + |C_3|^2 + |C_4|^2$, so Eq. (B1) is easily integrated:

$$\tan(\Theta) = \tan(\Theta_0)\exp(a\Gamma z). \tag{B4}$$

To obtain a complete solution one must determine Θ_0 and Θ_d in terms of boundary values. To this end, using the expressions for $|Q_d| + |Q_0|$ and $|Q_d| - |Q_0|$ from Eqs. (B3) and (B4), one forms a system of three algebraic equations (for Θ_d, Θ_0, and a). The solution is of the form

$$\tan(u) = \frac{q}{b - v}, \tag{B5a}$$

$$\tan(s) = \frac{qb}{wb - c}, \tag{B5b}$$

$$b \sin(u) = aI \sin(s), \tag{B5c}$$

where $u = \Theta_d - \Theta_0$, $s = \Theta_d + \Theta_0$, $q = \overline{C}_2C_3 + C_1\overline{C}_4 + \text{c.c.}$, $b = aI \coth(a\Gamma/2)$, $v = |C_4|^2 - |C_3|^2 + |C_2|^2 - |C_1|^2$, $w = |C_4|^2 + |C_3|^2 - |C_2|^2 - |C_1|^2$, $p = \overline{C}_2C_3 - C_1\overline{C}_4 + \text{c.c.}$, and $c = pq - wv$. The self-consistency requirement on this solution leads to an equation for a:

$$b^2q^2 + (wb - c)^2 = a^2I^2[q^2 + (b - v)^2]. \tag{B6}$$

Equation (B6) must be solved numerically. However, a good approximate solution is obtained if one notes that a should lie between -1 and 1. In fact, $a = 0$ is always a (trivial) solution of Eq. (B6). For sufficiently large Γ (positive or negative) one obtains a nonzero (positive or negative) value for a. This defines the coupling strength threshold for oscillation. Assuming $a\Gamma$ to be small, one obtains $b = 2I/\Gamma$ and

$$a = \frac{1}{I}\left[\frac{4I^2q^2 + (2Iw - c\Gamma)^2}{(q\Gamma)^2 + (2I - v\Gamma)^2}\right]^{1/2}. \tag{B7}$$

A few numerical and approximate solutions are presented in Fig. 2. Having found a, $\tan(\Theta_d + \Theta_0)$, and $\tan(\Theta_d - \Theta_0)$, one can easily determine Θ_0 and Θ_d.

APPENDIX C: NUMERICAL ALGORITHM FOR PHOTOREFRACTIVE WAVE-MIXING EQUATIONS

To the spatial problem at hand we apply a simple spectral method. We consider just one of Eqs. (1) and one transverse dimension x, as an example. The equation is first Fourier transformed:

$$(\partial_z + i\beta k - i\phi k^2)\tilde{A}_1(z) = \widetilde{QA}_4(z), \tag{C1}$$

where $k = k_x$ denotes the transverse part of the wave vector and the tilde denotes the spatial Fourier transform, which is easily achieved by use of a fast-Fourier-transform algorithm. In Eq. (C1), only the dependence on the relevant marching variable (z) is retained. The initial partial differential equation is thus transformed into a system of first-order ordinary differential equations, with as many equations as there are Fourier components. These equations cannot be solved exactly, because of the convolution $\widetilde{QA}_4$. However, a formal solution can be written down:

$$\tilde{A}_1(z) = \exp[i(\phi k^2 - \beta k)z] \times \left\{\tilde{A}_1(0) + \int_0^{z'} \widetilde{QA}_4(z')\exp[-i(\phi k^2 - \beta k)z']\mathrm{d}z'\right\} \tag{C2}$$

or, if integration is performed over a δz step:

$$\tilde{A}_1(z+\delta z) = \exp[i(\phi k^2 - \beta k)\delta z]\tilde{A}_1(z) + \exp[i(\phi k^2 - \beta k)(z+\delta z)] \int_z^{z+\delta z} \widetilde{QA}_4(z') \times \exp[-i(\phi k^2 - \beta k)z']\mathrm{d}z' . \quad \text{(C3)}$$

The influence of the convection term β is now clear: It leads to a lateral shift of the fields. Numerically this equation can be treated to different orders of accuracy and algorithmic sophistication. We opt for the simplest and computationally least expensive approximation. We assume that the term $\widetilde{QA}_4$ does not change appreciably across the (presumably small) integration step. In doing so, we keep in mind that DPC is a high-gain process. In such a process saturation is easily achieved, and the region of rapid change of fields is localized inside the crystal. Hence the approximation appears to be better than its linear δz dependence (cf. Fig. 3). Equation (C3) is now integrated:

$$\tilde{A}_1(z+\delta z) = \exp[i(\phi k^2 - \beta k)\delta z]\tilde{A}_1(z) + i\widetilde{QA}_4(z)\,\frac{1-\exp[i(\phi k^2 - \beta k)\delta z]}{\phi k^2 - \beta k}, \quad \text{(C4)}$$

and the field $A_1(z+\delta z)$ advanced for a δz step is determined by an inverse spatial Fourier transform. In this manner the crystal (spatial) integration loop is formed: the fields A_1 and A_4 advance from $z=0$, starting with appropriate initial profiles (usually Gaussian), and likewise A_2 and A_3 fields "advance" backward from $z=d=1$. Along the way, the values of total intensity I and $q(t) = A_1\overline{A}_4 + \overline{A}_2 A_3$ are collected, to be used in the temporal integration loop.

Once the crystal integration loop is completed and the relevant quantities are calculated, one advances the grating amplitude for a time step δt. Although one can think of more-sophisticated algorithms, it is clear that Eq. (4) can be treated similarly to the spatial equation in the inverse space. As a first-order ordinary differential equation, it can be formally integrated:

$$Q(t) = \exp\left(-\frac{\eta t}{\tau}\right)\left[Q(0) + \Gamma\int_0^t \frac{q(t')}{I(t')}\exp\left(\frac{\eta t'}{\tau}\right)\frac{\mathrm{d}t'}{\tau}\right]. \quad \text{(C5)}$$

Assuming that $q(t)/I(t)$ is approximately constant across the (small) time interval, one obtains

$$Q(t+\delta t) = \exp\left(-\frac{\eta\delta t}{\tau}\right)Q(t) + \Gamma\frac{q(t)}{\eta I(t)}\left[1-\exp\left(-\frac{\eta\delta t}{\tau}\right)\right]. \quad \text{(C6)}$$

This formula is easily discretized. Again, the accuracy is low (linear in δt). However, as mentioned above, the temporal change of q (and I) is rather gradual, and by an appropriate choice of $\delta t/\tau$ satisfactory results are obtained. (In our computations $\delta t/\tau$ is always less than 0.1. The parameter η, if real, is of the same order of magnitude.)

ACKNOWLEDGMENTS

This research project has financial support from the Sonderforschungsbereich 185 "Nichtlineare Dynamik" of the Deutsche Forschungsgemeinschaft. J. Leonardy thanks O. Hess, M. Münkel, and M. Sauer for many fruitful discussions. We thank one of the reviewers for thoughtful comments on our paper.

REFERENCES AND NOTES

1. M. Cronin-Golomb, B. Fischer, J. O. White, and A. Yariv, "Theory and applications of four-wave mixing in photorefractive media," IEEE J. Quantum Electron. **QE-20,** 12–30 (1984).
2. B. Fischer, S. Sternklar, and S. Weiss, "Photorefractive oscillators," IEEE J. Quantum Electron. **25,** 550–569 (1989); S. Sternklar, S. Weiss, M. Segev, and B. Fischer, "Beam coupling and locking of lasers using photorefractive four-wave mixing," Opt. Lett. **11,** 528–530 (1986); S. Weiss, S. Sternklar, and B. Fischer, "Double phase-conjugation: analysis, demonstration, and applications," Opt. Lett. **12,** 114–116 (1987).
3. A. A. Zozulya, "Double phase-conjugate mirror is not an oscillator," Opt. Lett. **16,** 545–547 (1991); V. V. Eliseev, V. T. Tikhonchuk, and A. A. Zozulya, "Double phase-conjugate mirror: two-dimensional analysis," J. Opt. Soc. Am. B **8,** 2497–2504 (1991).
4. N. V. Bogodaev, V. V. Eliseev, L. I. Ivleva, A. S. Korshunov, S. S. Orlov, N. M. Polozkov, and A. A. Zozulya, "Double phase-conjugate mirror: experimental investigation and comparison with theory," J. Opt. Soc. Am. B **9,** 1493–1498 (1992).
5. A. A. Zozulya, M. Saffman, and D. Z. Anderson, "Propagation of light beams in photorefractive media: fanning, self-bending, and formation of self-pumped four-wave-mixing phase conjugation geometries," Phys. Rev. Lett. **73,** 818–821 (1994); "Double phase-conjugate mirror: convection and diffraction," J. Opt. Soc. Am. B **12,** 255–264 (1995).
6. M. Segev, D. Engin, A. Yariv, and G. C. Valley, "Temporal evolution of photorefractive double phase-conjugate mirrors," Opt. Lett. **18,** 1828–1830 (1993); S. Orlov, M. Segev, A. Yariv, and G. C. Valley, "Conjugation fidelity and reflectivity in photorefractive double phase-conjugate mirrors," Opt. Lett. **19,** 578–580 (1994); D. Engin, M. Segev, S. Orlov, and A. Yariv, "Double phase conjugation," J. Opt. Soc. Am. B **11,** 1708–1717 (1994).
7. K. D. Shaw, "The double phase conjugate mirror is an oscillator," Opt. Commun. **90,** 133–138 (1992).
8. A. Yariv, *Quantum Electronics*, 2nd ed. (Wiley, New York), Chap. 6, p. 112.
9. The situation has changed considerably since this paper was submitted for publication. A number of treatments have appeared and are listed in Refs. 5, 6, and 10.
10. M. Cronin-Golomb, "Whole beam method for photorefractive nonlinear optics," Opt. Commun. **89,** 276–282 (1992); K. Ratnam and P. P. Banerjee, "Nonlinear theory of two-beam coupling in a photorefractive material," Opt. Commun. **107,** 522–530 (1994).
11. S. R. Liu and G. Indebetouw, "Spatiotemporal patterns and vortices dynamics in phase conjugate resonators," Opt. Commun. **101,** 442–455 (1993).
12. W. Krolikowski, M. R. Belić, M. Cronin-Golomb, and A. Bledowski, "Chaos in photorefractive four-wave mixing with a single interaction region," J. Opt. Soc. Am. B **7,** 1204–1209 (1990).
13. J. V. Moloney, M. R. Belić, and H. M. Gibbs, "Calculation of transverse effects in optical bistability using fast Fourier transform techniques," Opt. Commun. **41,** 379–382 (1982); M. Lax, G. P. Agrawal, M. R. Belić, B. J. Coffey, and W. L. Louisell, "Electromagnetic field distribution in loaded unstable resonators," J. Opt. Soc. Am. A **2,** 731–742 (1985).
14. M. R. Belić and M. Petrović, "Unified method for solution of wave equations in photorefractive media," J. Opt. Soc. Am. B **11,** 481–485 (1994).

15. M. R. Belić, J. Leonardy, D. Timotijević, and F. Kaiser, "Transverse effects in double phase conjugation," Opt. Commun. **111,**99–104 (1994).
16. N. Wolffer, P. Gravey, J. V. Moisan, C. Laulan, and J. C. Launay, "Analysis of double phase conjugate mirror interaction in absorbing photorefractive crystals: application to BGO:Cu," Opt. Commun. **73,** 351–356 (1989); N. Wolffer and P. Gravey, "High quality phase conjugation in a double phase conjugate mirror using InP:Fe at 1.3 μm," Opt. Commun. **107,** 115–119 (1994).
17. F. T. Arecchi, "Space-time complexity in nonlinear optics," Physica D **51,** 450–464 (1991); F. T. Arecchi, S. Boccaletti, G. Giacomelli, G. P. Puccioni, P. L. Ramazza, and S. Residori, "Space–time chaos and topological defects in nonlinear optics," Physica D **61,** 25–39 (1992).
18. W. Krolikowski and B. Luther-Davies, "The effect of a high external electric field on a photorefractive ring phase conjugator," Appl. Phys. B **55,** 180–182 (1992).